Molecular BioSystems

COMMUNICATION

View Article Online
View Journal | View Issue

Cite this: *Mol. BioSyst.*, 2016, 12, 1110

Received 15th January 2016,
Accepted 9th February 2016

DOI: 10.1039/c6mb00033a

www.rsc.org/molecularbiosystems

Protonation state of $F_{420}H_2$ in the prodrug-activating deazaflavin dependent nitroreductase (Ddn) from *Mycobacterium tuberculosis*†

A. Elaaf Mohamed,[a] F. Hafna Ahmed,[a] Sundaram Arulmozhiraja,[a] Ching Y. Lin,[a] Matthew C. Taylor,[b] Elmars R. Krausz,[a] Colin J. Jackson*[a] and Michelle L. Coote*[ac]

The protonation state of the deazaflavin dependent nitroreductase (Ddn) enzyme bound cofactor F_{420} was investigated using UV-visible spectroscopy and computational simulations. The reduced cofactor $F_{420}H_2$ was determined to be present in its deprotonated state in the holoenzyme form. The mechanistic implications of these findings are discussed.

The discovery of cofactor F_{420} (Fig. 1), and a new family of F_{420}-dependent enzymes, in a wide range of Actinobacteria, including pathogenic mycobacteria,[1–4] has led to increased interest in F_{420} dependent oxidoreductases (FDORs). The absence of F_{420} dependent biochemical reactions in humans, and their prevalence in *Mycobacterium tuberculosis* (TB), the causative agent of tuberculosis, has made the enzymes that depend on and synthesize this cofactor drug targets for new treatments of the disease.[5] Bicyclic nitroimidazoles have recently been discovered to be activated by a class of FDORs called FDORAs,[2,4,6] which are thought to have a physiological role in reducing oxidative stress against mycobacteria during infection.[7] Bicyclic nitroimidazoles show anti-mycobacterial effects such as respiratory poisoning and the disruption of cell wall biosynthesis.[8,9] One of these compounds, pretomanid (formerly PA-824) shown in Fig. 1, is currently in clinical trials and shows promising results against multi-drug resistant strains of TB.[10]

In order to exert its anti-mycobacterial activity against *M. tuberculosis*, pretomanid must initially be reduced by the protein encoded by rv3547, referred to as the Deazaflavin-dependent nitroreductase (Ddn), in concert with reduced cofactor F_{420} ($F_{420}H_2$).[1,6,11] This reaction results in the formation of three stable metabolites, one of which decomposes to nitric oxide (NO) and results in anaerobic anti-mycobacterial activity.[1]

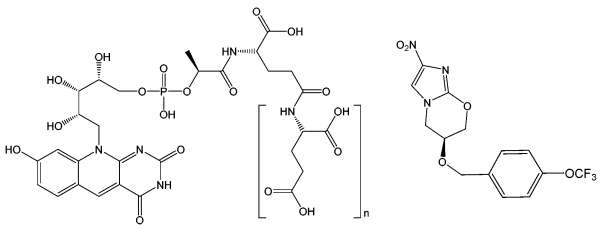

Fig. 1 Structures of F_{420} (left) and pretomanid (right).

Although the role of both Ddn and F_{420} in the activity of pretomanid is known,[1,6,8,11] the precise catalytic mechanism is not fully understood. Thus, a better understanding of this reaction and the configuration and protonation state of the reactants within the enzyme's active site is essential to further improving this class of anti-mycobacterial pro-drugs.

While the deazaflavin F_{420} is structurally analogous to riboflavin based cofactors such as flavin mononucleotide (FMN) and flavin adenine dinucleotide (FAD), it is functionally closer to nicotinamide (*e.g.* NAD) cofactors by being involved in redox reactions as a hydride carrier involved in two electron transfer mechanisms.[12] Consistent with its involvement in redox reactions, F_{420} exists in both oxidized (F_{420}) and reduced ($F_{420}H_2$) forms, as shown in Fig. 2. The oxidized cofactor exhibits strong and distinct UV-visible spectroscopic properties, with a characteristic absorbance peak at 420 nm that is different to the spectroscopic properties of the reduced species.[13] This allows for the study of F_{420} dependent reactions using UV/vis spectroscopy to follow changes in the amounts of the oxidized cofactor being formed or consumed.[1,4,6,7,11] These spectroscopic properties are also sensitive to pH changes, with the structural changes due to deprotonation of the 8-OH and 1-NH groups in the oxidized and reduced species (Fig. 2), respectively, influencing the absorbance bands.

The protonation state of the cofactor will significantly influence the catalytic mechanism owing to the availability or unavailability of labile hydrogens. However, in the current literature this has not been addressed and $F_{420}H_2$ is often presented as its neutral species.[6] In this study we have determined

[a] *Research School of Chemistry, The Australian National University, Canberra, ACT 2601, Australia. E-mail: colin.jackson@anu.edu.au, michelle.coote@anu.edu.au*
[b] *CSIRO Land and Water, Black Mountain Laboratories, Canberra, ACT 2601, Australia*
[c] *ARC Centre of Excellence for Electromaterials Science*

† Electronic supplementary information (ESI) available. See DOI: 10.1039/c6mb00033a

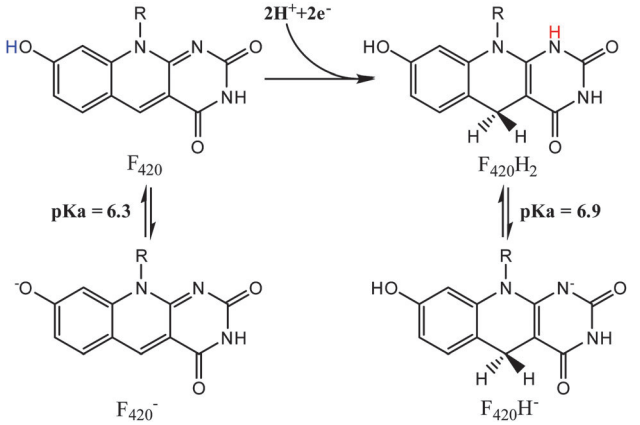

Fig. 2 The protonated and deprotonated species of F_{420} (left) and $F_{420}H_2$ (right).[14]

the protonation state of F_{420} and $F_{420}H_2$ when bound to Ddn, and a homolog of Ddn from *Mycobacterium smegmatis*, MSMEG_2027, using a combination of UV-visible spectroscopy and time-dependent density functional theory (TD-DFT) calculations.[4] Initially, absorbance spectra of both F_{420} and $F_{420}H_2$ were measured in an aqueous environment as a function of pH so as to assign the neutral and deprotonated spectra (Fig. 3; Fig. S1 in ESI†). However, in order to ensure that these assignments do not change in the lower polarity environment within the enzyme active site, we also used TD-DFT to calculate the neutral and deprotonated spectra under both aqueous and low polarity solvent environments (Fig. 4).

For F_{420}, the characteristically intense absorbance peak at 420 nm gives way to a weaker peak at 400 nm at lower pH values with the observed pK_a of 6.5 (Fig. 3a) agreeing with previously reported values of 6.3.[14,15] The spectroscopic red-shift from 400 to 420 nm is also indicative of stabilization of the π–π^* transitions stemming from the deprotonation of the 8-OH group. For $F_{420}H_2$, its characteristic peak at 320 nm did not exhibit the strong red-shift upon deprotonation observed in F_{420}, instead it was the neutral species that was slightly red-shifted to 322 nm with the deprotonated species at 319 nm and consistent with literature for both F_{420} as well as the structural analogue 1,5-dihydrodeazariboflavin.[15,16] Rather, a more noticeable spectral change is seen at 260 nm with a peak present in the deprotonated species. Both the 320 nm and 260 nm peaks exhibit a pK_a near neutrality at 7.1 (Fig. 3b). These results agree with previously published literature values for $F_{420}H_2$ of 6.9 and 7.2 for $F_{420}H_2$ and 1,5-dihydrodeazariboflavin.[15,16]

Although the computationally derived electronic transitions for both species deviated from the experimental values, their relative values, and the trends that are observed, agree closely with the experimental spectrum (Fig. 4). For both species it was also noted that the electronic transitions responsible for the absorbance peaks remained in agreement for both the aqueous environment with a dielectric constant ε = 80.1 and the low polarity environment with ε = 12. This uniform behaviour enables us to directly compare experimental UV-visible spectra of the cofactor in aqueous conditions with that of when the

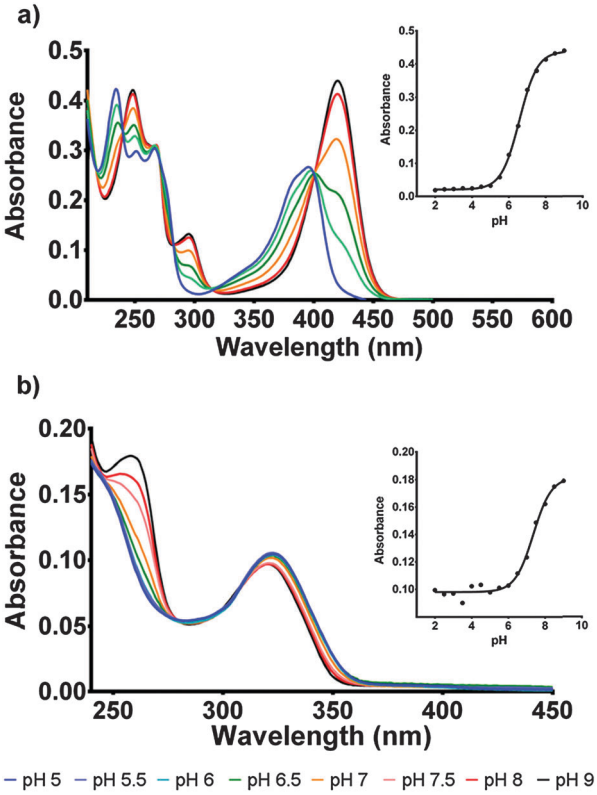

Fig. 3 (a) pH curve of F_{420} for the pH range of 5–9 showing the spectroscopic changes observed with pH change. Inset: The curve of absorbance change at 420 nm across the pH range which determined the pK_a for deprotonation was 6.5. (b) pH curve of $F_{420}H_2$ for pH range 5–9 with associated spectroscopic changes. Inset: The curve of absorbance change at 260 nm across the pH range which determined the pK_a for deprotonation was 7.1.

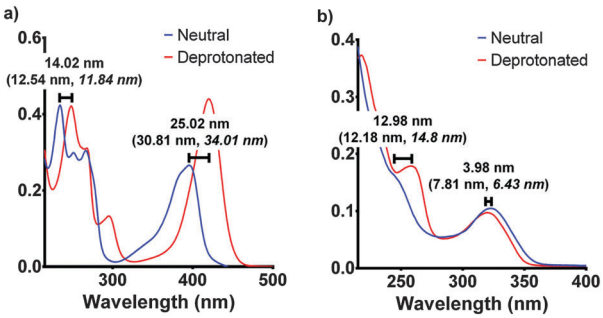

Fig. 4 The experimental spectroscopic peak shifts for F_{420} (a) and $F_{420}H_2$ (b) compared with the calculated values (in parenthesis) for both aqueous and low polarity (in italics). The experimental results are those for pH 5 and pH 9 for neutral and deprotonated respectively. The electronic transitions were calculated using the ωB97XD/6-311+G(2d,p) level of theory in Gaussian 09.[17,18]

cofactor is bound within the active site to complete the holoenzyme. The full comparisons of the simulated electronic transitions with experiment are in Fig. S2 in ESI.†

To determine the protonation state in the enzyme, the bound absorbance spectrum was measured with $F_{420}H_2$ bound to the Ddn and 2027 enzymes (Fig. 5; Fig. S4 in ESI†). The results

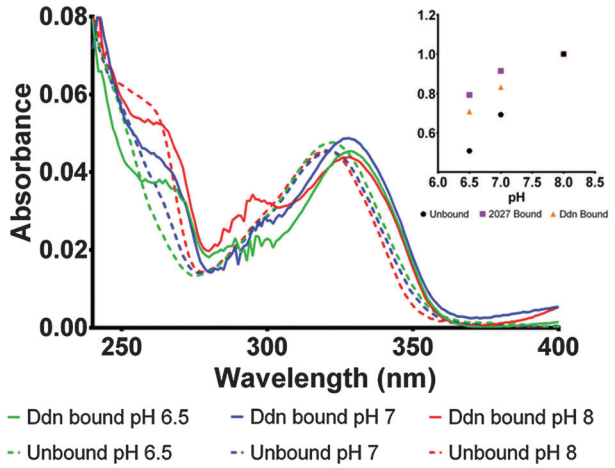

Fig. 5 Comparison of the Ddn bound $F_{420}H_2$ absorbance spectra at different pH with the unbound aqueous species. The spectroscopic features are red-shifted by approximately 5–10 nm due to further stabilization from binding. The assignment of the protonation state can be made due to the presence of the 260 nm peak at both pH 7 and pH 6.5 which is absent in the aqueous spectra. The inset demonstrates the increase in absorbance (at 262 nm) at pH 6.5, 7 and 8 for both Ddn and 2027 bound when compared with the aqueous conditions. The values were normalised at pH 8 to account for concentration fluctuations.

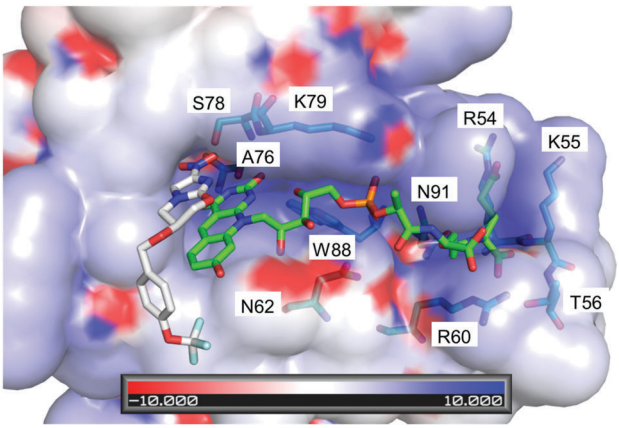

Fig. 6 Crystal structure of F_{420} bound within Ddn (PDB ID: 3R5R), with the substrate pretomanid docked *via* simulation.[4,6] The electrostatics of the surrounding residues reveals the positively charged surroundings which help bind and stabilize the negatively charged deprotonated cofactor. The residues that contribute to the positive environment are shown and labelled. Scale is in kT/e.

identified the cofactor as being stabilized more in its deprotonated state even at neutral pH where the conversion usually takes place. Upon binding to the enzyme active site, the electronic transitions that give rise to the absorbance spectrum are stabilized due to electrostatic interactions with the surrounding amino acid residues leading to most spectroscopic features being red-shifted by approximately 5–10 nm. This observation proved to be a convenient indicator for whether the species being measured was actually bound to the active site or only present in the surrounding environment.

Owing to the limited spectroscopic changes at the 320 nm peak associated with the deprotonation, the secondary 260 nm peak, which exhibits greater differences between the two states, was used to determine the species present. At pH 8, where the cofactor is normally deprotonated in aqueous solution, no change was observed as both bound and unbound $F_{420}H_2$ exhibited the deprotonated peak at 260 nm. However, at pH 7 where the 260 nm peak is greatly diminished under aqueous conditions as it is shifted to the neutral state, the bound spectrum still shows a notable contribution of the 260 nm peak indicating the presence of the deprotonated species. Furthermore, the comparison of the bound spectrum at pH 6.5 and unbound spectrum at pH 6.5 corroborate this assessment as the 260 nm deprotonated peak is still observed at pH values below the (aqueous) pK_a in the bound species while, as expected, is completely absent under aqueous conditions. On this basis we can conclude that the cofactor $F_{420}H_2$ is bound and stabilized within the active site in its deprotonated form.

This same observation is made using the experimental spectra of $F_{420}H_2$ bound to the Ddn homolog MSMEG_2027 (Fig. S4 in ESI†), which shares a similar active site structure.[4] Fig. 6 displays a docking simulation of the cofactor and substrate within the active site, which shows how the deprotonated species might be stabilized by the surrounding positively-charged electrostatic environment.

Correctly assigning the protonation state of $F_{420}/F_{420}H_2$ is essential for further mechanistic studies involving the cofactor $F_{420}H_2$ and Ddn. This result suggests that the proton transfer step of the reaction, which completes the $2H^+/2e^-$ reduction, has to be facilitated *via* a source other than from the cofactor. Additionally, the deprotonation of the reduced cofactor enables it to readily form the more stable neutral molecule F_{420} following the hydride transfer instead of a less stable carbocation that would result if the protonated species were involved. There are several ionisable sidechains in the vicinity of the cofactor that could act as general acids in this reaction; their potential involvement is currently under investigation. Conversely, it has also been suggested that the protonation of pretomanid is completed by water molecules from the surrounding environment.[1] A proposed mechanism utilizing deprotonated $F_{420}H_2$ is presented in Fig. 7, where initial hydride transfer is followed by a proton transfer event. These steps result in the formation of oxidized F_{420}, and reduced pretomanid-H_2, which then undergoes heterolytic bond cleavage and bond formation to produce the anti-mycobacterial nitric oxide species.

The holoenzyme structure solved by Cellitti *et al.* was obtained with the oxidized species F_{420} at pH 6.5.[6] Therefore the cofactor would be deprotonated, as would be true for $F_{420}H_2$ at physiological pH: both molecules would lack the N1 hydrogen, although the hydroxyl group at C8 would most likely be deprotonated in F_{420}. Since the C8–OH group extends into the solvent, this difference is unlikely to significantly affect substrate binding, making the crystal structure a good model for the holoenzyme structure. Our results provide some insight into the substrate specificity of Ddn since the substrate range would be relatively broad if the proton transferred to C2 could be donated by $F_{420}H_2$. Instead, because the proton appears to be donated from a side-chain or protein-stabilized water

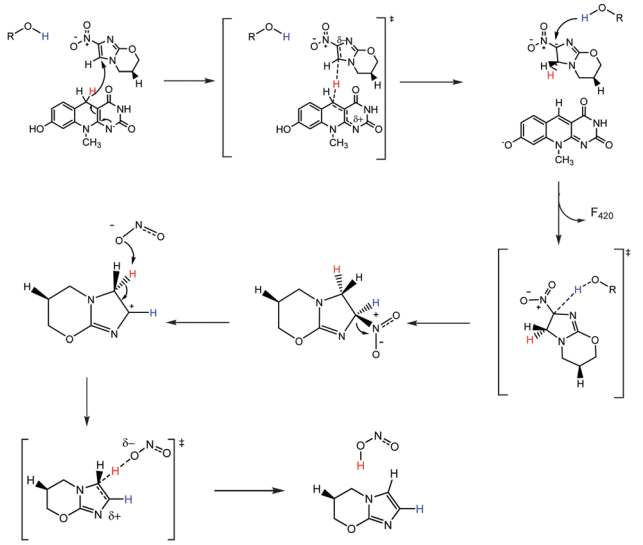

Fig. 7 Proposed mechanism for the activation reaction of pretomanid by $F_{420}H_2$. The R group signifies the possibility of the proton source for being a tyrosine residue, serine residue or a water molecule and is currently under investigation.

molecule, there are significant constraints on the substrate range, given that the substrates must be in sufficiently close contact with the general acid for proton transfer to occur. This model is consistent with previous work that showed there is little enantioselectivity with smaller pretomanid analogs, such as CGI-17341 and phenyl oxazole, since the C2 atom will be in the same approximate position in either enantiomer.[11]

In summary, we determined the protonation state of the cofactor $F_{420}H_2$ when bound to the Ddn active site. This has a significant impact on our understanding of the $F_{420}H_2$ mediated activation mechanism as it implies that maintaining the deprotonated state of $F_{420}H_2$ contributes to the catalytic efficiency of the enzyme and that the proton source to complete the reaction is not $F_{420}H_2$ itself, but a separate residue or nearby molecule involved within the active site.

MLC and CJJ gratefully acknowledge funding from the Australian Research Council in the form of Discovery Project funding (DP130102144) and ARC Future Fellowships. MLC also acknowledges generous allocations of supercomputing time on the National Facility of the Australian National Computational Infrastructure.

Notes and references

1 R. Singh, U. Manjunatha, H. I. M. Boshoff, Y. H. Ha, P. Niyomrattanakit, R. Ledwidge, C. S. Dowd, I. Y. Lee, P. Kim, L. Zhang, S. Kang, T. H. Keller, J. Jiricek and C. E. Barry, *Science*, 2008, **322**, 1392–1395.
2 M. C. Taylor, C. J. Jackson, D. B. Tattersall, N. French, T. S. Peat, J. Newman, L. J. Briggs, G. V. Lapalikar, P. M. Campbell, C. Scott, R. J. Russell and J. G. Oakeshott, *Mol. Microbiol.*, 2010, **78**, 561–575.
3 L. Daniels, N. Bakhiet and K. Harmon, *Syst. Appl. Microbiol.*, 1985, **6**, 12–17.
4 F. H. Ahmed, P. D. Carr, B. M. Lee, L. Afriat-Jurnou, A. E. Mohamed, N.-S. Hong, J. Flanagan, M. C. Taylor, C. Greening and C. J. Jackson, *J. Mol. Biol.*, 2015, **427**, 3554–3571.
5 J. D. Selengut and D. H. Haft, *J. Bacteriol.*, 2010, **192**, 5788–5798.
6 S. E. Cellitti, J. Shaffer, D. H. Jones, T. Mukherjee, M. Gurumurthy, B. Bursulaya, H. I. Boshoff, I. Choi, A. Nayyar, Y. S. Lee, J. Cherian, P. Niyomrattanakit, T. Dick, U. H. Manjunatha, C. E. Barry III, G. Spraggon and B. H. Geierstanger, *Structure*, 2012, **20**, 101–112.
7 M. Gurumurthy, M. Rao, T. Mukherjee, S. P. S. Rao, H. I. Boshoff, T. Dick, C. E. Barry and U. H. Manjunatha, *Mol. Microbiol.*, 2013, **8**, 744–755.
8 C. K. Stover, P. Warrener, D. R. VanDevanter, D. R. Sherman, T. M. Arain, M. H. Langhorne, S. W. Anderson, J. A. Towell, Y. Yuan, D. N. McMurray, B. N. Kreiswirth, C. E. Barry and W. R. Baker, *Nature*, 2000, **405**, 962–966.
9 U. Manjunatha, H. I. M. Boshoff and C. E. Barry, *Commun. Integr. Biol.*, 2009, **2**, 215–218.
10 R. Dawson, A. H. Diacon, D. Everitt, C. van Niekerk, P. R. Donald, D. A. Burger, R. Schall, M. Spigelman, A. Conradie, K. Eisenach, A. Venter, P. Ive, L. Page-Shipp, E. Variava, K. Reither, N. E. Ntinginya, A. Pym, F. von Groote-Bidlingmaier and C. M. Mendel, *Lancet*, 2015, **385**, 1738–1747.
11 M. Gurumurthy, T. Mukherjee, C. S. Dowd, R. Singh, P. Niyomrattanakit, J. A. Tay, A. Nayyar, Y. S. Lee, J. Cherian, H. I. Boshoff, T. Dick, C. E. Barry and U. H. Manjunatha, *FEBS J.*, 2012, **279**, 113–125.
12 C. Walsh, *Acc. Chem. Res.*, 1986, **19**, 216–221.
13 P. Cheeseman, A. Toms-Wood and R. S. Wolfe, *J. Bacteriol.*, 1972, **112**, 527–531.
14 L. M. de Poorter, W. J. Geerts and J. T. Keltjens, *Microbiology*, 2005, **151**, 1697–1705.
15 L. D. Eirich, G. D. Vogels and R. S. Wolfe, *Biochemistry*, 1978, **17**, 4583–4593.
16 R. Spencer, J. Fisher and C. Walsh, *Biochemistry*, 1976, **15**, 1043–1053.
17 J.-D. Chai and M. Head-Gordon, *Phys. Chem. Chem. Phys.*, 2008, **10**, 6615–6620.
18 M. J. Frisch, *et al.*, *Gaussian 09, Rev D.01*, Gaussian Inc., Wallingford CT, 2009.